RSC Advances

ROYAL SOCIETY OF CHEMISTRY

www.rsc.org/advances

Journal Name

RSCPublishing

ARTICLE

Enhanced thermoelectric performance of BiSbTe-based composites incorporated with amorphous Si_3N_4 nanoparticles

Cite this: DOI: 10.1039/xoxxoooooox

Received ooth January 2012,
Accepted ooth January 2012

DOI: 10.1039/xoxxoooooox

www.rsc.org/

Y.C. Dou, X.Y. Qin*, D. Li, Y.Y. Li, H.X. Xin, J. Zhang, Y.F. Liu, C.J. Song and L.Wang

Thermoelectric properties of BiSbTe-based composites dispersed with small amount (<1 vol.%) of amorphous Si_3N_4 (a-Si_3N_4) nanoparticles (~25nm) were investigated in the temperature range from 303K to 483K. The results indicate that with a-Si_3N_4 content increasing, the thermopower (S) of the a-Si_3N_4/BiSbTe composites increases substantially at T<~370K, due to the decreased carrier concentrations and the enhanced energy-dependent scattering of carrier at the heterojunction potential. Simultaneously, a-Si_3N_4 nanodispersion causes ~20-30% reduction in thermal conductivity (κ) owing to phonon scattering of nanoparticles as well as phase boundaries. As a result, high dimensionless figure of merit (ZT) values of up to 1.20 (~303K) and 1.38 (~383K) are obtained in $Bi_{0.4}Sb_{1.6}Te_3$ incorporated with only 0.44 vol.% a-Si_3N_4 nanoparticles, demonstrating that thermoelectric performance of BiSbTe alloy can be improved effectively through incorporation of a-Si_3N_4 nanoparticles.

Introduction

Thermoelectric (TE) materials have attracted increasing attention owing to their potential applications in energy conversion and power generation.[1] The efficiency of TE materials is characterized by the dimensionless figure of merit ZT, which is defined as $ZT=S^2\sigma T/\kappa$ ($\kappa=\kappa_L+\kappa_C$), where S, σ, κ,(κ_L, κ_C) and T are the Seebeck coefficient (or thermopower), electrical conductivity, thermal conductivity (the lattice κ_L and carrier κ_C contributions), and absolute temperature respectively.[2-3] It is clear that there are usually two ways to improve ZT: one is to boost the power factor PF ($S^2\sigma$) and the other is to reduce thermal conductivity (κ). Although there have been persistent efforts to improve ZT values since the 1950s, ZT of the best commercial materials has remained 1 mainly due to the interdependence of the parameters involved in ZT.[4] However, with the development of experimental and theoretical innovation several successful examples have been reported recently, in which remarkable advances in ZT can be realized by decoupling the electrical and thermal transport properties.[5-8] Up to now, the main approach is to introduce different nanostructures into bulk TE materials by in-situ precipitation or incorporation of nanoparticles, in which phonons are effectively scattered while the scattering of conducting electrons is minimized. For instance, enhanced thermoelectric properties have been achieved in both p-type and n-type half-Heuslers by Ren et al.[9] In fact, the notable improvement in ZT value, benefited from the formation of half-Heusler nanocomposite through a high energy ball milling.[9-10] Obviously, the significant increase of Seebeck coefficient and the remarkable reduction of phonon thermal conductivity are believed to be due to quantum effect[11]/energy filtering effect[12] at the interface and size effect of the nanostructures, respectively, thereby providing a significant ZT enhancement.

Bi_2Te_3-based alloys are the state-of-the-art thermoelectric materials that are (uniquely) used commercially at near room temperature for refrigeration. Numerous researches have been performed to improve their ZT by structural and composition modification since Bi_2Te_3-based alloys were found in 1960s[13-18]. Especially, the ZT value as high as 1.4 (at ~373K)[17] or even 1.50 (at ~390K)[18] was reported in p-type $Bi_xSb_{2-x}Te_3$ with nanostructures. Previous studies, such as D-ATP/BiSbTe[19] (ZT_{max}=1.3 at 420K), SiC/BiSbTe[20] (ZT_{max}=1.33 at 373K), indicated that incorporating nanoparticles into BiSbTe matrix could bring positive impact on improving its ZT.

In order to reduce lattice thermal conductivity and enhance thermopower of BiSbTe system, small amounts (<1vol.%) of amorphous Si_3N_4 (a-Si_3N_4) nanoparticles (~25nm) were incorporated into BiSbTe matrix to form nanocomposites in the present work. Nanometer sized a-Si_3N_4 (~25nm) is a kind of insulator that can form fine dispersed nanophase in BiSbTe matrix, and phase boundaries and the heterojunction potential are expected to be formed in the composite system, which could be beneficial to enhancing both phonon scattering and selective carrier scattering, respectively. Besides, as a constituent of the composite system, the disordered amorphous structure of a-Si_3N_4 could lead to a further thermal conductivity reduction by enhancing phonons scattering due to the extremely small mean free paths of phonons in a-Si_3N_4. As expected, our results show that incorporating a-Si_3N_4 nanoparticles into the p-type BiSbTe matrix is effective for its thermoelectric property enhancement. Specifically, incorporation of only 0.44vol.% a-Si_3N_4 nanoparticles into $Bi_{0.4}Sb_{1.6}Te_3$ alloy results in remarkably decrease in thermal conductivity (κ), leading to higher dimensionless figure of merit (ZT) value of up to 1.20 (~303K) and 1.38 (~383K), respectively. Present results suggest that incorporation of amorphous nanoparticles into BiSbTe-based alloys be an effective way to enhancing their thermoelectric performance.

Experimental procedures

Elemental powders Bi (99.99%, Alfa Aesar), Sb (99.5%, Sigma Aldrich) and Te (99.999%, Alfa Aesar) granules were weighted according to the formula of $Bi_{0.4}Sb_{1.6}Te_3$ doped with 3wt% Te. The powder mixture was loaded into quartz ampoule sealed under vacuum at 10^{-2} Pa, and then heated to 800℃ for 24h. Then the ingot was grinded into powders. These powders were subjected to ball milling process with the compositions of $Bi_{0.4}Sb_{1.6}Te_3$ (BiSbTe) and blended with a volume fraction f (f=0, 0.22, 0.44, 0.88vol.%) of commercial a-Si_3N_4 nanoparticles (the purity is ≥99.0 atm.% and mean particle size is ~25nm) in a planetary ball mill at 150 rpm for 6h in a purified argon atmosphere. Stainless steel vessels and agate balls were used. The weight ratio of ball to powder was kept at 30:1. Proper ethyl alcohol was needed in order to gain good dispersed composites. After oven dry, the ball-milled powders were compacted by spark plasma sintering under a pressure of 50 MPa in a diameter of 20 mm graphite mold in vacuum for 5 min. The sintering temperature and heating rate were 673 K and 323 K/min, respectively. Disks of 10 mm in diameter and 2 mm thick were then obtained. The phase structure was studied by X-ray diffraction at room temperature using Cu Ka radiation. The fractographs were observed by field emission scanning electron microscopy (FE-SEM). The compositions of the composites were confirmed by using energy dispersive analysis system of X-ray (EDX) equipped in FE-SEM.

Bars of about 2×2×10 mm and Disks of 9 mm in diameter and 2 mm thick were cut from the pressed disks and polished for the thermoelectric properties characterization. The electrical resistivity and the Seebeck coefficient were measured simultaneously by commercial equipment (ULVAC-RIKO: ZEM-3, Japan) under He atmosphere from 303 to 483 K. Hall coefficient was measured at 303 K by applying a field of 250 mT, and the carrier concentrations and mobility were calculated by using Hall coefficient and electrical resistivity. The thermal diffusivity, D, was measured using the laser flash method (Netzsch, LFA 457). The specific heat, C_p, was determined by a commercial instrument (Pyris Diamond DSC, Perkine Elmer).The density, γ, was measured by the Archimedes method. The resulting total thermal conductivity was calculated from the measured thermal diffusivity D, specific heat C_p, and density γ from the relationship $\kappa = D\gamma C_p$.

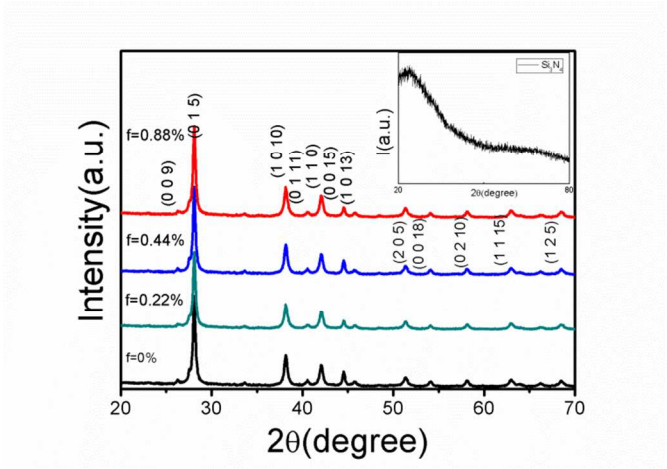

Fig.1. XRD patterns of f(a-Si_3N_4)/BiSbTe composite powders (f=0, 0.22, 0.44 and 0.88 vol.%) and of a-Si_3N_4 nanoparticles.

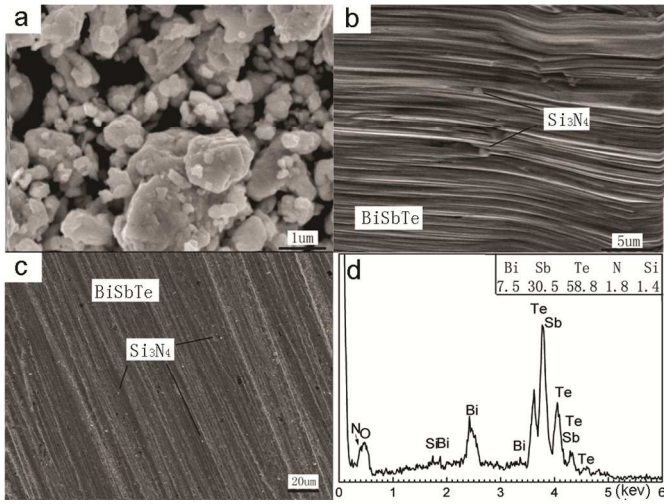

Fig.2. SEM images of composite powders (a), the vertical section (b), the horizontal cross section (c) and the electron energy spectrum (d) obtained by using EDX for f(a-Si_3N_4)/BiSbTe (f=0.44vol.%) composite sample.

Results and discussion

Microstructural characterization

Fig.1 shows the XRD patterns of f(a-Si_3N_4)/BiSbTe (f=0, 0.22, 0.44 and 0.88vol.%) composite powders. The diffraction peaks of Si_3N_4 powder are shown in the inset of Fig.1, revealing that Si_3N_4 nanoparticles are amorphous. All the main diffraction peaks in the XRD patterns of f(a-Si_3N_4)/BiSbTe composites are consistent with the standard JCPDS (PDF#01-072-1836) card of $Bi_{0.4}Sb_{1.6}Te_3$ with rhombohedral structure (crystal group R3m). As compared with the pattern of BiSbTe, no obvious changes are observed in XRD patterns for f(a-Si_3N_4)/BiSbTe composites, for the dispersed a-Si_3N_4 nanoparticles have amorphous structure which cannot give rise to any diffraction peak. The SEM images and the electron energy spectrum obtained by using EDX for 0.44vol.% a-Si_3N_4/BiSbTe composite sample are shown in Fig.2. As shown in Fig.2(a), the grain size of BiSbTe powder range from around 0.2μm to 2μm, and some very small white grains existed. The vertical and horizontal cross-sections of scanning electron micrographs of the 0.44vol.% a-Si_3N_4/BiSbTe composite sample are given in Fig.2(b) and Fig.2(c), respectively. It can be seen that fine-grained microstructure can be expected due to the low sintering temperature and fast sintering process of SPS technique. Moreover, one can observe some very small white particles distributed homogeneously in BiSbTe matrix, indicating that a-Si_3N_4 nanoparticles are successfully incorporated in BiSbTe matrix, forming (a-Si_3N_4)/BiSbTe bulk composites, which can be confirmed by the electron energy spectrum obtained by using EDX as shown in Fig.2(d).

Thermoelectric properties

The electrical properties of f(a-Si_3N_4)/BiSbTe (f=0, 0.22, 0.44 and 0.88vol.%) composite samples are shown in Fig.3. As shown in Fig.3(a), electrical resistivity ρ (1/σ) of all the samples increases with increasing temperature, showing the characteristics of

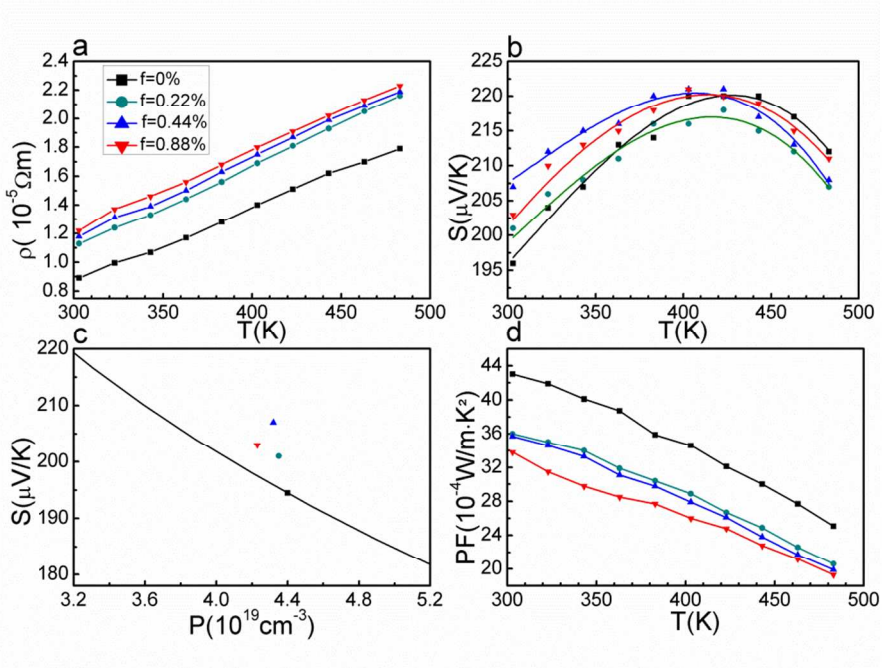

Fig.3. The temperature dependence of ρ (*a*), S (b), PF (d) and Variation of S with p (c) for *f*(*a*-Si_3N_4)/BiSbTe composite samples (*f*=0, 0.22, 0.44 and 0.88 vol.%) at 303 K. The solid line is Pisarenko relation for BiSbTe.

Table 1 The Hall coefficient Rh, carrier concentrations *P*, Hall mobility μ, electrical resistivity ρ, the scattering parameter λ for *f*(*a*-Si_3N_4)/BiSbTe composite samples with different *a*-Si_3N_4 content *f* at 303 K

f	Rh(10^4cm^3/C)	P(10^{19} cm^{-3})	μ(cm^2/Vs)	ρ(10^{-3}Ω·cm)	λ
0	1.42	4.41	158.9	0.892	0
0.22vol.%	1.43	4.35	127.1	1.13	0.07
0.44vol.%	1.45	4.32	122.6	1.18	0.13
0.88vol.%	1.48	4.23	121.1	1.22	0.06

degenerate semiconducting behavior. Since *a*-Si_3N_4 is a kind of insulator that has a very high electrical resistivity, ρ of these composites increases with increasing *f*. Generally, ρ at 303K increases from 0.892×10^{-3}Ω·cm to 1.13×10^{-3}Ω·cm, 1.18×10^{-3}Ω·cm and 1.22×10^{-3}Ω·cm, respectively, as shown in table 1. The positive values of Seebeck coefficient (S) (Fig.3(b)) in the whole temperature range mean that the major charge carriers in all the samples are holes. In addition, S for the composite samples was observed to increase with increasing temperature, and after reaching a maximum value it decreases obviously with further increase in temperature. This behavior has been reported previously[21] and could be attributed to thermal excitation of minority carriers. Moreover, S generally increases with increasing *a*-Si_3N_4 content (*f*=0.22, 0.44vol.%) below ~370K. Specifically, S for 0.44vol.% *a*-Si_3N_4/BiSbTe composite sample at 303K reaches 207μV/K, which is higher than that (196μV/K) of the BiSbTe matrix. Nevertheless, for the large amount addition of *a*-Si_3N_4 (*f*=0.88vol.%), S of the composite sample lowers as compared to that of the sample with *f*=0.44vol.%.

Hall coefficient measurement indicates that as *f* increases the carrier concentrations p decreases slightly due to insulator nature of *a*-Si_3N_4, as given in table 1. Simultaneously, the carrier mobility μ declines from 158.9 cm^2/Vs to 127.1, 122.6, and 121.1 cm^2/Vs with increasing *f*, due to enhanced interface scattering. Hence, it is clear now that the increase of ρ is caused by the decrease of both p and μ in the composites. Generally, for degenerate semiconductors S can be expressed by the Mott equation, as following:

$$S = \frac{\pi^2\kappa_B^2 T}{3q}\left[\frac{\partial \ln(\sigma(E))}{\partial E}\right]_{E=E_f} = \frac{\pi^2\kappa_B^2 T}{3q}\left[\frac{1}{p}\frac{\partial p(E)}{\partial E}+\frac{1}{\mu}\frac{\partial \mu(E)}{\partial E}\right]_{E=E_f} \quad (1)$$

with carrier mobility $\mu(E)=q\tau/m_d^*$, where k_B, q, σ, p, τ, m_d^* and E_f are Boltzmann constant, carrier charge, electrical conductivity, carrier concentration, relaxation time, effective mass of carrier and Fermi energy, respectively. if the bands have a parabolic energy-momentum E(k) dispersion relation, the density of states $g(E) \propto E^{1/2}$, and the relaxation time τ(E) for carriers usually has power form with energy E^{22}, i.e. $\tau(E)=\tau_0 E^{\lambda-1/2}$. Then, formula (1) can be expressed as:

$$S = \frac{\pi^2\kappa_B^2 T}{3q}\left[\frac{\partial p(E)}{p\partial E}+\frac{\lambda-\frac{1}{2}}{E}\right]_{E=E_f} \quad (2)$$

where λ is carrier scattering parameter. One knows from formula (2) that S can be elevated via the decrease of p or via the increase of λ. An increase in λ means that carriers with lower energies are scattered preferentially (due to the relation $\tau(E)=\tau_0 E^{\lambda-1/2}$)[23] and S is enhanced due to this energy filtering effect[22,23]. In order to investigate whether energy filtering effect plays a role in the enhancement of S for our composite samples, λ is calculated based on the experimental data of p and S by using a single parabolic band

model. In this model, effective mass m_d* and S can be expressed as[24]:

$$m_d^* = \frac{h^2}{2k_B T}\left(\frac{p}{4\pi F_{1/2}(\xi_F)}\right)^{2/3} \quad (3)$$

$$S = \frac{k_B}{e}\left[\frac{(\lambda+2)F_{\lambda+1}(\xi_F)}{(\lambda+1)F_\lambda(\xi_F)} - \xi_F\right] \quad (4)$$

with Fermi integral of order *i*

$$F_i(\xi_F) = \int_0^\infty \frac{x^i}{1+e^{(x-\xi_F)}}dx \quad (5)$$

where *h* the Planck constant and ξ_F is the reduced Fermi level $F_f/(k_BT)$. In our calculations, we use $m_d^*=1.60m_e$ (which is consistent with literature values[25]) and assume acoustic phonon scatting (λ=0) for the BiSbTe matrix. Then, the calculated λ for *f*(*a*-Si_3N_4)/BiSbTe composite samples is shown in table 1. One can see that, λ increases from 0 to 0.07, 0.13 and 0.06 in the composites as *f* increases, respectively, indicating enhancement of energy filtering effect. And it can be seen that the optimal sample is 0.44 vol.%(*a*-Si_3N_4)/BiSbTe, which has the biggest scattering parameter λ=0.13. The Fig.3(c) shows the Pisarenko relation (solid line) for the BiSbTe

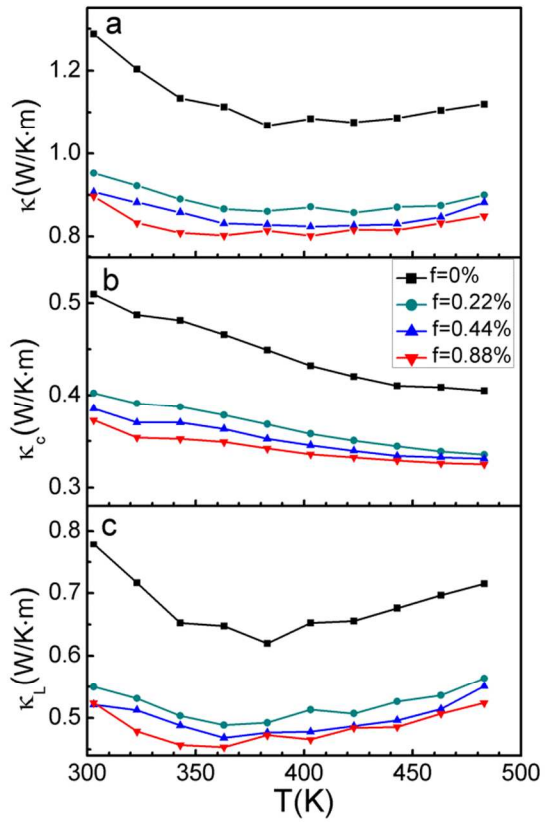

Fig.4. Variation of the total thermal conductivity κ (*a*), the carrier thermal conductivity κ_c (b) and the lattice thermal conductivityκ_L (c) with temperature for *f*(*a*-Si_3N_4)/BiSbTe composite samples (*f*=0, 0.22, 0.44 and 0.88 vol.%).

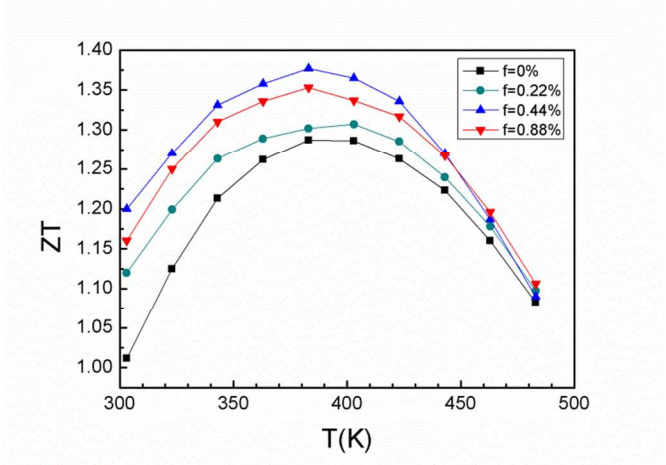

Fig.5. ZT values with temperature for *f*(*a*-Si_3N_4)/BiSbTe composite samples (*f*=0, 0.22, 0.44 and 0.88 vol.%).

matrix and the S values (at 303K) for all the samples, which indicates that further enhancement of S for the composite samples is obtained due to the enhanced energy-dependent scattering of carrier at the heterojunction potential. According to the above analysis, one can find that the increase in S is caused both by the decrease in *p* and the enhancement in λ.

As shown in Fig.3(d), the maximum value of power factor (PF) of 43 $\mu Wcm^{-1}K^{-1}$ is obtained for the BiSbTe matrix at 303 K, and PF of all the samples decreases with increasing temperature. Moreover, the PF values of these composite samples decrease with increasing *f*. For instance, When *f* increases to 0.44vol%, its PF decreases to 35.7 $\mu Wcm^{-1}K^{-1}$ at 303 K, which is almost 17% lower than that of the BiSbTe matrix. The decrease in PF mainly comes from reduction in σ (1/ρ).

Fig.4 shows that the temperature dependence of the total thermal conductivity (κ), the carrier thermal conductivity (κ_C) and the lattice thermal conductivity (κ_L) for *f*(*a*-Si_3N_4)/BiSbTe (*f*=0, 0.22, 0.44 and 0.88vol.%) composite samples, respectively. One can see from Fig.4(a), the temperature behavior of the total thermal conductivity for the four samples is similar: it decreases with increasing temperature and then increases with further increasing temperature. Moreover, κ for all the composite samples is smaller than that of the BiSbTe matrix and decreases with increasing *f* in the whole temperate range. Specially, κ for 0.44vol.% *a*-Si_3N_4/BiSbTe is reduced to 0.91 $WK^{-1}m^{-1}$ at 303K, which is about 30% lower than that (1.29 $WK^{-1}m^{-1}$) of the BiSbTe matrix. The total thermal conductivity consists of a lattice thermal conductivity κ_L and a contribution of mobile charge carriers, κ_c, i.e.$\kappa=\kappa_L+\kappa_c$. Usually, κ_c can be estimated by the Wiedemann-Franz law ($\kappa_C = \frac{L_0 T}{\rho}$), where $L_0 = 1.5\times10^{-8}\,V^2/K^2$ is the Lorentz number, which is obtained from fitting the Seebeck data to the reduced chemical potential[19,26], T is the temperature in Kelvin. As shown in Fig.4(b), κ_c in the whole temperature range investigated decreases with increasing *f*, which is originated from the increase in ρ. By comparison of Fig.4(c) with Fig.4(a), one finds that the smaller total thermal conductivity with increasing *f* originates mainly from the reduction in its lattice thermal conductivity κ_L. It can be seen that κ_L decreases monotonically with increasing *f* in the whole temperate

range, which can be attributed to enhanced phonon scattering by the incorporated nanoparticles and the phase boundaries. Specifically, κ_L of $f(a\text{-}Si_3N_4)$/BiSbTe (f=0.44vol.%) at 303K reaches 0.52 $WK^{-1}m^{-1}$, which is around 33% lower than that (0.78 $WK^{-1}m^{-1}$) of the BiSbTe matrix. However, the increase in κ_L with temperature at T>~363-483K could be ascribed to the ambipolar contribution due to the increasing intrinsic excitation. In the intrinsic conduction region for narrow-band-gap semiconductors, such as BiSbTe system, a considerable contribution to the thermal conductivity is made by the component due to the ambipolar diffusion of electrons and holes.[27] In this case, the total thermal conductivity κ is given by $\kappa=\kappa_L+\kappa_c+\kappa_{bi}$ (ambipolar contribution); then at high temperatures (T>~363-483K) $\kappa-\kappa_c=\kappa_L+\kappa_{bi}$, which suggest κ_L shown in Fig.4(c) included contribution of κ_{bi}.

Based on the data obtained above, Fig.5 gives the ZT values for $f(a\text{-}Si_3N_4)$/BiSbTe (f=0, 0.22, 0.44 and 0.88vol.%) composite samples as functions of temperature. It can be seen that ZT values of all the samples increase with increasing temperature, and after reaching a maximum value ZT decreases with further increasing temperature. Moreover, with increasing $a\text{-}Si_3N_4$ content to f=0.22 and 0.44vol.%, ZT increase significantly. Nevertheless, for the large amount addition of $a\text{-}Si_3N_4$ (f=0.88vol.%), ZT of the composite sample lowers as compared to that of the sample with f=0.44vol.%, due to its much smaller PF. Overall, ZT for all the composite samples is larger than that of the BiSbTe matrix in the whole temperate range. Specifically, ZT of the composite sample with f=0.44vol.% is 1.20 at 303K, larger than that (1.01) of BiSbTe matrix in the present study; its maximum ZT reaches 1.38 at 383K. The large enhancement of ZT for all the composite samples originates from the significantly reduced thermal conductivity and enhanced energy filtering effect owing to incorporation of $a\text{-}Si_3N_4$ nanoparticles.

Conclusions

Composites $f(a\text{-}Si_3N_4)$/BiSbTe (f=0, 0.22, 0.44 and 0.88vol.%) were prepared, and their thermoelectric properties were studied at temperatures from 303 to 483K. The results indicate that although electrical resistivity increases with increasing $a\text{-}Si_3N_4$ content due to the decrease in both carrier concentrations and carrier mobility, Seebeck coefficient increases substantially at T<~370K owing to decrease in carrier concentrations and increase in scattering parameter. Specially, incorporation of $a\text{-}Si_3N_4$ nanoparticles into BiSbTe significantly reduces the thermal conductivity of composite samples due to enhanced phonon scattering by the nanoparticles and the phase boundaries. As a result, ZT of $f(a\text{-}Si_3N_4)$/BiSbTe with f=0.44vol.% reaches 1.20 at 303K (which is larger than that (1.01) of BiSbTe matrix in the present study), and specifically its maximum ZT reaches 1.38 at 383K, which is round 8% larger than that (1.28) of BiSbTe matrix. Present results suggest that incorporation of amorphous nanoparticles into thermoelectric materials, such as BiSbTe-based alloys, be an effective way to enhancing their thermoelectric performance.

Acknowledgements

Financial support from the National Natural Science Foundation of China (Nos. 11374306, 11174292, 51101150, 50972146, and 10904144) are gratefully acknowledged.

Notes and references

* Key Laboratory of Materials Physics, Institute of Solid State Physics Chinese Academy of Sciences, 230031 Hefei, P. R. China. E-mail: xyqin@issp.ac.cn；Tel:+86 0551 65592750; fax:+86 0551 65591434

1 D. M. Rowe, *CRC Handbook of Thermoelectrics* .CRC Press, LLC, 1995.
2 T. M. Tritt, *Semiconductors and semimetals, recent trends in thermoelectric materials research:part one to three.* San Diego, CA: Aca-demic, 2000.
3 G. J. Snyder, *Appl. Phys. Lett.*, 2009, **94**, 102111.
4 T. C. Harman, P. J. Taylor, M. P. Walsh, B. E. LaForge, *Science*, 2002, **297**, 2229.
5 A. J. Minnich, M. S. Dresselhaus, Z. F. Ren and G. Chen, *Energy Environ. Sci.*, 2009, **2**, 466.
6 M. S. Dresselhaus, G. Chen, M. Y. Tang, R. Yang, H. Lee, D. Wang, Z. F. Ren, J. Fleurial, and P. Gogna, Adv. Mater., 2007, **19**, 1043.
7 T. C. Harman, M. P. Walsh, B. E. LaForge, and G. W. Turner, *J. Electron. Mater.*, 2005, **34**, L19 .
8 I. Boukai, Y. Bunimovich, J. Tahir-Kheli, J. K. Yu, W. A. Goddard, and J.R. Heath, *Nature*, 2008,**451**, 168.
9 W.S. Liu, X. Yan, G. Chen,, Z.F. Ren, *Nano Energy*, 2012, **1**, 42.
10 X. Yan, G. Joshi, W.S. Liu, Y.C. Lan, H. Wang, S.Y. Lee,J.W. Simonson, S.J. Poon, T.M. Tritt, G. Chen, Z.F. Ren, *Nano Letters*, 2011,**11**,556.
11 T. E. Humphrey and H. Linke, *Phys. Rev. Lett.*, 2005, **94**, 096601.
12 J. Martin, L. Wang, L. Chen and G. S. Nolas, *Phys. Rev. B*, 2009, **79**, 115311.
13 R. Venkatasubramanian, E. Siivola, T. Colpitts, and B. O' Quinn, *Nature*, 2001, **413(6856)**, 597.
14 D. Y. Chung, T. Hogan, P. Brazis, and R. L. Melissa, *Science*, 2000, **287**, 1024.
15 J. Seo, K. Park, D. Lee, *C. Lee, Mater. Lett.*, 1998, **35**, 4.
16 C. J. Liu, H. C. Lai, Y. L. Liu, and L. R. Chen, *J. Mater. Chem.*, 2012, **22**, 4825.
17 B. Poudel, Q. Hao, Y. Ma, Y. C. Chen, A. Minnich, B. Yu, X. Yan, D. Z. Wang, A. Muto, D. Vashaee, X. Y. Chen, J. M. Liu, M. S. Dresselhaus, G. Chen, and Z. F. Ren, *Science*, 2008, **320**, 634.
18 W. J. Xie, J. He, H. J. Kang, X. F. Tang, S. Zhu, M. Laver, S. Y. Wang, J. R. D. Copley, C. M. Brown, Q. J. Zhang, and T. M. Tritt, *Nano Lett.*, 2010, **10**, 3283.
19 T. Zhang, J. Jiang, Y. K. Xiao, Y. B. Zhai, S. H. Yang, G. J. Xu, and Z. F. Ren, *RSC Adv.*, 2013, **3**, 4951.
20 J.H. Li , Q. Tan , J.F. Li , D.W.Liu , F. Li , Z.Y. Li , M.M. Zou ,and K. Wang, *Adv. Funct. Mater.*, 2013, **10**, 1002.
21 D. H. Kim, C. Kim, S. H. Heo, and H. Kim, *Acta Mater.*, 2011, **59**, 405.
22 X. H. Yang, X. Y. Qin, J. Zhang, D. Li, H. X. Xin, and M. Liu, *J. Alloys. Compd.,* 2013, **558**, 203.
23 J. P. Heremans, C. M. Thrush, and D. T. Morelli, *Phys. Rev. B*, 2004, **70(11)**, 115334.
24 T. Caillat, J. P. Fleurial, and A. Borshchevsky, *J. Phys. Chem. Solids*, 1997, **58(7)**, 1119.
25 S. V. Ovsyannikov, Yu. A. Grigor'eva, G. V. Vorontsov, L. N. Luk'yanova, V. A. Kutasov, and V. V. Shchennikov, *Physics of the Solid State*, 2012, **54**, 261.
26 K. Biswas, J. Q. He, I. D. Blum, C. Wu, T. P. Hogan, D. N. Seidman, V. P. Dravid, and M. G. Kanatzidis, *Nature*, 2012, **489**, 414.
27 L. D. Zhao, H. J. Wu, S. Q. Hao, C. I. Wu, X. Y. Zhou, K. Biswas, J. Q. He, T. P. Hogan, C. Uher, C. Wolverton, V. P. Dravid and M. G. Kanatzidis, *Energy Environ. Sci*.,2013, **6**, 3346.